CARBON letters

Original Articles
Carbon Letters Vol. 27, 72-80 (2018)

Comparative study on carboxylated styrene butadiene rubber composites reinforced by hybrid fillers of rice bran carbon and graphite carbon

Yuan Fan[1], Qingyuan Li[1], Xiangxu Li[1], Dam hee Lee[1] and Ur Ryong Cho[1,2,♠]

[1]School of Energy, Materials and Chemical Engineering, Korea University of Technology and Education, Cheonan 31253, Korea
[2]Research Center of Eco-friendly & High-performance Chemical Materials, Cheonan 31253, Korea

Article Info
Received 23 October 2017
Accepted 18 December 2017

♠Corresponding Author
E-mail: urcho@koreatech.ac.kr
Tel: +82-041-560-1340

Open Access
DOI: http://dx.doi.org/10.5714/CL.2018.27.072

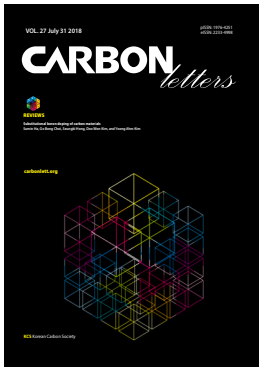

http://carbonlett.org

pISSN: 1976-4251
eISSN: 2233-4998

Abstract

In the present work, a comparative study of the mechanical behavior of two series of elastomeric composites, based on carboxylated styrene butadiene rubber (X-SBR) and reinforced with rice bran carbon (RBC) and graphite, is reported. Hybrid composites of X-SBR filled with RBC-graphite were also investigated in terms of the cure characteristics, hardness, tensile properties, abrasion resistance, and swelling. It was observed that the cure times decreased with the incorporation of a carbon filler whereas the torque difference, tensile strength, tensile modulus, hardness, and swelling resistance increased compared to the neat X-SBR revealing a favorable characteristic of crosslinking. Dynamic rheological analysis showed that the G' values of the composites, upon the addition of RBC-graphite, were changed to some extent. This demonstrates that the presence of a strongly developed network of fillers will ensure a reinforcing characteristic in a polymer matrix.

Key words: rice bran carbon, graphite, mechanical properties, composites, carboxylated styrene butadiene rubber

1. Introduction

The incorporation of a filler into elastomeric materials can improve reinforcement, processability, and economic benefits. Fillers are used as one of the most significant additives in the rubber industry. The reinforcement efficiency depends greatly on the particle size and surface area of the fillers [1]. Carbon fillers, especially carbon black as a reinforcing filler, are widely used to enhance the physical and mechanical properties of rubber vulcanizates [2]. Although carbon black is still commonly used in the rubber industry, it is produced from petroleum which results in high energy consumption and environmental problems. Consequently, the use of other carbon fillers as alternatives for reinforcing rubber is currently being investigated.

Various fillers such as carbon nanotubes [3], carbon fibers [4], and SiC [5] have been added to polymer composites, which meet the needs for practical applications of polymer composites. Among these, graphene and graphene oxide have been found to be a significant reinforcing material due to their high mechanical strength, nano size effects, and unique physical properties [6,7]. Moreover, much attention has been given to the fabrication of graphene-based nanoparticle hybrids fillers offering additional unique physicochemical properties and functions compared to the use of either material alone [8]. As reported in the literature, Lin et al. [9] fabricated silica/reduced graphene oxide hybrids via an electrostatic assembly, which was incorporated into styrene butadiene rubber to enhance the mechanical performances of the composites. Song and Zhang [10] showed in their study that carbon nanotube/reduced graphene oxide hybrid simultaneously enhanced the thermal conductivity and mechanical properties of styrene-butadiene rubber. Lin et al. [11] used graphene as a reinforcement filler for fabricating rubber composites and studied the effect of ZnO nanoparticles doped graphene on the mechanical properties of natural rubber com-

posites. Varghese et al. [12] used unfunctionalized few layer graphene nanoplatelets and carbon black as fillers and compared the effects of its hybrid fillers on the reinforcement of acrylonitrile butadiene rubber. More recently, Mondal and Khastgir [13] reported on hybrid composites of acrylonitrile butadiene that were filled with graphene nanoplatelets-carbon black and graphene nanoplatelets-multiwall carbon nanotubes which have a strong synergistic effect on the properties of the composites.

Although considerable research involving graphene-filled hybrid composites and graphene functionalized composites has been reported regarding the enhancement of the mechanical properties of rubber composites, most of this work was performed on graphene-based materials [14,15]. Carbon/carbon composites with tailorable thermal and mechanical properties are currently receiving much interest as a unique class of materials for various applications in a wide variety of fields [16]. Graphite, as the precursor of graphene oxide, is naturally abundant and oil-independent. However, reports on the reinforcing ability of graphite-based hybrid filler systems in rubber are scarce. Therefore, efforts should be made toward developing graphite as a reinforcing filler for rubber along with other carbon fillers. Additionally, driven by concerns for environmental pollution, oil resource depletion, sustainability in manufacturing, and lack of resources, it has been a challenge for the rubber industry to improve the performance of composites by only using environment-friendly reinforcing fillers derived from renewable resources. As a result, rice bran carbon (RBC), as a sustainable and green filler, is derived from agriculture residue because it is an efficient, low cost carbon source which is rich in both carbon as well as carbon black. It can be used as an eco-friendly filler in rubber and is expected to have good mechanical properties as well.

Carboxylated styrene butadiene rubber (X-SBR) has many unique properties, such as good processability, high binding force, and favorable aging resistance, which make it one of the most important polymers in terms of versatility and application. Using a latex compounding method can improve the dispersion of a filler while solving the problem of incompatibility between the rubber and the fillers. This method can be done easily and can be used to prepare high-performance composites [17]. In the present work, X-SBR composites incorporated with RBC and graphite were fabricated by a latex compounding method. RBC and graphite were used as fillers to improve the mechanical properties of X-SBR. Additionally, a comparative study was done on the effect of the hybrid filler systems in which RBC was used as the main filler and coupled with graphite as a secondary filler. The effects of the graphite loading on the various properties, cure characteristics, hardness, abrasion resistance, tensile properties, and swelling resistance of the X-SBR vulcanizates were systematically studied.

2. Experimental

2.1. Materials

X-SBR latex KSL 103 was provided by the KumHo Petrochemical Company, Korea. RBC with a particle size of 53 μm was obtained from the Sanwa-yushi Company, Japan. Graphite (flake type) with a particle size of under 5 μm was purchased from the Eport Trading Co., Korea. The other reagents were all available commercially in Korea, including zinc oxide, stearic acid, n-cyclohexyl-2-benzothiazole sulfonamide (CBS), sulfur, and 2,2'-dibenzothiazolyl disulfide (DD).

2.2. Preparation of the X-SBR composites

The X-SBR/RBC composites were fabricated by a latex compounding method. The X-SBR latex and RBC aqueous suspension were directly compounded with vigorous stirring for a given period to achieve a well-dispersed suspension. Then, the mixed emulsion was immediately co-coagulated using a 0.5% $CaCl_2$ solution. Thereafter, the product was dried in an oven at 60°C for 2 d. For comparison, the total filler content was kept constant at 30 phr (parts per hundred of rubber), and X-SBR latex filled with graphite was also prepared. Composites of the X-SBR with the hybrid fillers based on RBC and graphite at ratios of 25:5, 20:10, and 15:15 were prepared following a similar procedure, respectively. Finally, the X-SBR composites were compounded with rubber ingredients in an open two-roll mill and submitted to compression at 150°C for the optimum curing time examined by a rubber process analyzer (RPA). The sheet thickness of the compounds was about 2 mm and cut into specimens for the tensile test. The vulcanizates were designated as X-SBR/R_xG_y which represents the X-SBR composites containing x phr RBC and y phr graphite. For example, the abbreviation of X-SBR/$R_{25}G_5$ represents the composites filled with 25 phr RBC and 5 phr graphite. The basic formula of the composite is as follows (Table 1): X-SBR, 100 phr; zinc oxide, 5 phr; stearic acid, 1 phr; CBS, 2 phr; DD, 1.3 phr, and sulfur, 1.5 phr.

Table 1. X-SBR/RBC/graphite compound formulations

Ingredient phr[a)]	RBC	Graphite	Zinc oxide	Stearic acid	DD	CBS	Sulfur
X-SBR	0	0	5	1	1.3	2	1.5
X-SBR/R_{30}	30	0	5	1	1.3	2	1.5
X-SBR/$R_{25}G_5$	25	5	5	1	1.3	2	1.5
X-SBR/$R_{20}G_{10}$	20	10	5	1	1.3	2	1.5
X-SBR/$R_{15}G_{15}$	15	15	5	1	1.3	2	1.5
X-SBR/G_{30}	0	30	5	1	1.3	2	1.5

[a)]Parts per hundred of rubber.

2.3. Characterization

The ATR–FTIR spectra of the samples were recorded on a Perkin Elmer Spectrum 100S in the 4000–400 cm^{-1} region. The morphology of the fracture surfaces of the X-SBR composites was analyzed by SEM (JSM-7500 FE-SEM, JEOL, Japan). The dynamic rheological properties of the uncured compounds were measured with a rubber processing analyzer (RPA2000, Taiwan) to obtain the vulcanization properties of the rubber composites. The frequency and temperature were to 1.67 Hz and 60°C, respectively. The curing characteristics were determined at 150°C by the RPA. The curing rate index (CRI), which expresses the curing rate of rubber compounds, was calculated as follows:

$$CRI = \frac{100}{t_{90} - t_{s2}}$$

, where t_{90} and t_{S2} (min) are the optimum curing time and scorch time, respectively. The tensile tests of the X-SBR composites were measured using a Tinius Oisen (H5KT-0401) (according to ASTM D412) with a crosshead speed of 500 mm min^{-1} to obtain the mechanical properties. The shore A hardness of the specimens was tested with a Shore Durometer Type A (according to ASTM D2240). Abrasion tests were performed to measure wear loss with a Taber abrasion tester with a rotation speed of 80 r min^{-1} (according to ASTM D1044). The thermal properties of the composites were measured using a Perkin Elmer TGA 4000 by heating from 30 to 800°C at a rate of 20°C/min under a nitrogen flow of 20 cm^3 min^{-1}. The swelling degree of the vulcanized samples was measured through a swelling test. The weight of the specimens was determined after they were impregnated in toluene for 1, 2, 3, 6, 9, 12 and 24 h at room temperature. The equilibrium swelling ratio (S) of the composites was computed as follows:

$$S = \frac{(W_s - W_u)/\rho_s}{W_u/\rho_r} \times 100\%$$

, where W_s is the weight of the swollen specimens; W_u is the original weight of the specimens in air; ρ_s is the density of toluene (0.867 g cm^{-3}), and ρ_r is the density of the specimens.

3. Results and Discussion

3.1. ATR-FTIR analysis

The spectra of the RBC are shown in Fig. 1a. The broad peak at 3434 cm^{-1} was attributed to the stretching vibration of -OH. The peaks located at 2984, 2623, and 2283 cm^{-1} correspond with the C-H stretching vibration. A peak was observed at 1737 cm^{-1}, which belongs to the C=O stretching vibration. The bands at 1435 and 1364 cm^{-1} were associated with the C-H vibration, while the peak at 1213 cm^{-1} was assigned to C-O groups. The peaks at 1095 and 906 cm^{-1} were attributed to the characteristics of the Si-O-Si and Si-O bond, respectively. This suggests that the RBC is a carbon material which contains some functional groups. The spectrum of the graphite, which exhibited peaks at 3219, was related to -OH, whereas the peaks at 2605, 2178, and 2034 cm^{-1} were attributed to C-H (seen in Fig. 1b). The FTIR spectra of the X-SBR composites are compared in Fig. 1c. As for the X-SBR, the 2917 and 2842 cm^{-1} bands were due to the stretching vibration of the $-CH_2$, while the peak at 1738 cm^{-1} was associated with the C=O band. The peaks at 1600, 1500, and 1445 cm^{-1} were attributed to the C=C stretching bonds of the aromatic ring. Clearly, the X-SBR composites showed a similar backbone with different intensities, revealing the effect of the composition of the different hybrid fillers.

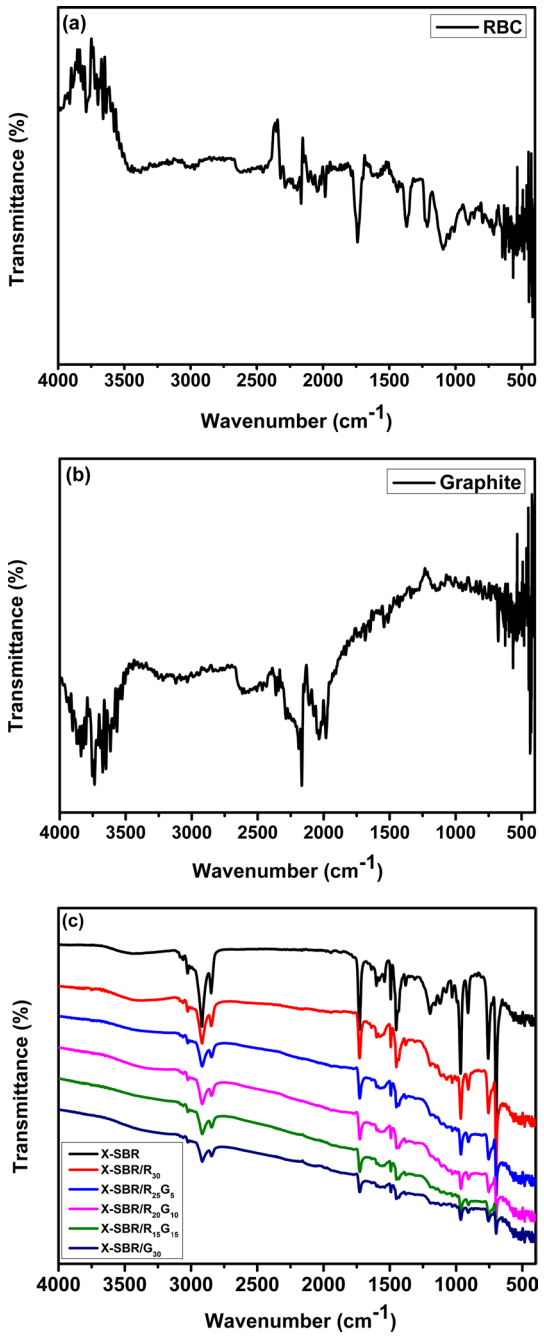

Fig. 1. FTIR spectra of the RBC (a), graphite (b), and X-SBR composites (c).

3.2. Fracture surfaces of the X-SBR composites

The tensile-fractured surfaces of the X-SBR composites were characterized by SEM images. As shown in Fig. 2a, the neat X-SBR has a relatively smooth surface. In contrast, a rough surface was observed in the X-SBR composites (seen in Fig. 2b-f), indicating the successful introduction of the carbonaceous fillers on the surface of the rubber matrix despite their slight aggregation. Regarding the X-SBR filled with the RBC and graphite hybrid fillers, as the graphite loading increased, more small graphite particles became embedded in the rubber matrix. Because of this, the X-SBR filled with the RBC and graphite hybrid fillers acquired a more uneven surface (seen in Fig. 2c-e), suggesting a strong interfacial adhesion between the filler and matrix. The morphologies of the pristine RBC and graphite are shown in Fig. 2g and h. The RBC particles have an irregular shape. As well documented, the average particle size of RBC was 15.2 μm [18]. Compared with RBC, spherical particles were observed in the graphite. Additionally, energy dispersion spectroscopy was used to analyze the elemental composition. RBC was derived from the carbonization of a mixture of rice bran and phenol resin (composed of carbon, oxygen, phosphorus and metallic elements), whereas the graphite had a high carbon content. This indicates that both fillers were carbon materials containing a high carbon element.

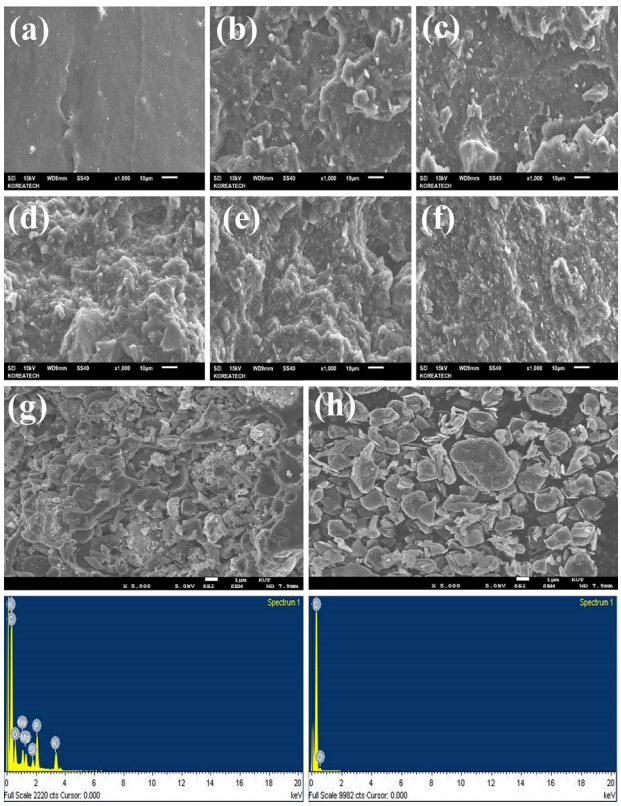

Fig. 2. SEM images of (a) X-SBR; (b) X-SBR/R_{30}; (c) X-SBR/$R_{25}G_5$; (d) X-SBR/$R_{20}S_{10}$; (e) X-SBR/$R_{15}G_{15}$; (f) X-SBR/G_{30}; (g) RBC particles, and (h) graphite particles.

3.3. Vulcanization characteristics

The vulcanization curves of the X-SBR composites are depicted in Fig. 3. As seen in Fig. 3, the scorch time (T_{s2}), optimum cure time (T_{90}), minimum torque (M_L) and maximum torque (M_H) were obtained in the X-SBR filled with RBC, graphite, and a hybrid filler of the two. The vulcanization properties of the X-SBR composites are listed in Table 2. The value of M_L during vulcanization increased when the graphite contents were increased in the hybrids of the RBC and graphite-filled X-SBR composites. This is attributed to the increased effective graphite contents enhanced by the interaction among the graphite particles. As shown in Table 2, the M_L and M_H of the neat X-SBR compounds were 2.84 and 9.24 N m, respectively. The incor-

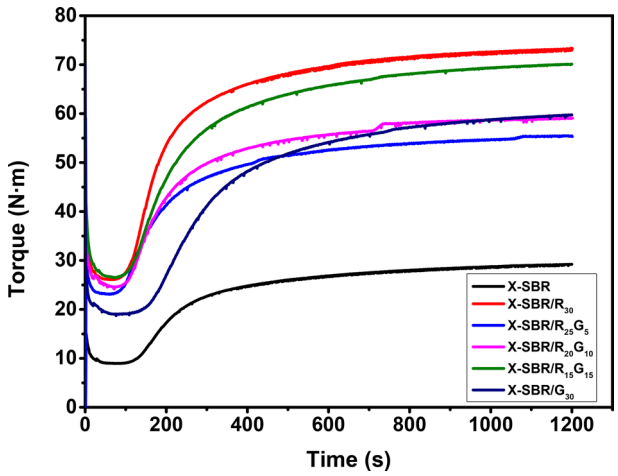

Fig. 3. Vulcanization curves of X-SBR, X-SBR/R_{30}, X-SBR/$R_{25}G_5$, X-SBR/$R_{20}S_{10}$, X-SBR/$R_{15}G_{15}$ and X-SBR/G_{30}.

Table 2. Vulcanization properties of the X-SBR/RBC/graphite composites

Sample	M_L (N m)	M_H (N m)	ΔH (N m)	t_{s2} (min)	t_{90} (min)	CRI (min^{-1})
X-SBR	2.84	9.24	6.4	3.03	10.88	12.74
X-SBR/R_{30}	8.26	23.18	14.92	2.12	8.85	14.86
X-SBR/$R_{25}G_5$	7.32	17.56	10.24	2.03	9.55	13.30
X-SBR/$R_{20}G_{10}$	7.74	18.70	10.96	2.23	9.92	13
X-SBR/$R_{15}G_{15}$	8.39	22.18	13.79	2.3	10.03	12.94
X-SBR/G_{30}	5.98	18.90	12.92	3.2	11.58	11.93

poration of RBC, graphite, and its hybrid filler into the X-SBR matrix increased the value of M_H compared to that of the unfilled X-SBR vulcanizates because of the absorption of the X-SBR chains onto the surface of the carbon. As was reported, M_H relied on chain entanglement and crosslink density [19]. The values of ΔH obtained were the difference between the M_L and M_H values, which represents the crosslink density of the cured compound. This result is indicative of the network that was formed by the filler, which can be used as an effective reinforcing filler. In addition, it was found that T_{90} increased as the graphite contents were increased because there were hydroxyl groups on the surface of the graphite powders, and vulcanizers were absorbed by the excess graphite. As a consequence, the curing rate was lowered during the vulcanization, which was consistent with an earlier report [20]. Generally, the crosslink density is optimum at T_{90} for most rubber composites, and the CRI values are inversely proportional to the difference between T_{90} and T_{s2}, indicating the curing rate of the composites. In this case, compared with the neat X-SBR, the value of the X-SBR composites containing RBC and graphite exhibited higher CRI values. However, as for X-SBR/$R_{15}G_{15}$, the value of CRI became lower. This was probably due to filler aggregation, which was caused by the resistance to the polymer chain mobility.

3.4. Mechanical properties

The mechanical properties of the X-SBR composites are shown in Fig. 4. From the stress-strain curves, the related parameters such as the modulus at 100% (MPa), tensile strength (MPa) and elongation at break (%) could be obtained (summarized in Table 3). For the neat X-SBR, its modulus at 100%, tensile strength and elongation at break were 1.83 MPa, 7.90 MPa and 465%, respectively. Compared with the neat X-SBR, the X-SBR/R_{30} exhibited reinforcements of the mechanical properties; this observation indicated that RBC can be used as a reinforcing filler due to its high carbon content. Meanwhile, the effect of the hybrid filler systems, X-SBR/$R_{25}G_5$, X-SBR/$R_{20}G_{10}$, and X-SBR/$R_{15}G_{15}$, was also studied in which RBC was used as the main filler and coupled with graphite as the secondary filler at different ratios. Although all of the samples did not exhibit a synergistic effect, the X-SBR filled with RBC and graphite hybrid fillers exhibited a higher reinforcement compared to the X-SBR/R_{30}. This suggests that the addition of graphite can further improve the mechanical properties of the X-SBR. From these results, the X-SBR/$R_{20}G_{10}$ showed a better reinforcing effect. Further increased proportions of graphite incorporated with RBC into the X-SBR resulted in a decrease in the tensile strength; this phenomenon can be explained by the situation in which the poor dispersion of small-sized particles at a higher filler concentration easily led to aggregation and weak interfacial bonding. For comparison, the mechanical properties of the X-SBR/G_{30} are also included. It was noted that the X-SBR/G_{30} showed a stronger reinforcing effect, proving that graphite has a greater reinforcement ability due to its higher carbon content and smaller particle size. In addition, another important observation was the rise in hardness of the X-SBR composites compared with the neat X-SBR. This was likely due to the incorporation of carbon materials in the soft matrix, reducing the elasticity of the X-SBR. This agrees with a report that the inclusion of a rigid phase is able to increase the polymer stiffness [21].

Additionally, the well-known Mooney–Rivlin equation was further used to analyze the connection between the tensile and strain behavior of the orientation of the rubber chains to obtain information about the interfacial interaction and the rubber network [22]. The equation can be expressed as follows:

$$\sigma^* = \frac{\sigma}{2\lambda - \frac{2}{\lambda^2}} = 2C_1 + \frac{2C_2}{\lambda}$$

, where σ is the tensile stress, and λ is the extension ratio. C_1 is directly proportional to the elastically active network chains per unit volume of the rubber, and C_2 is related to the number of elastically effective trapped entanglements and the number of steric obstructions and other network defects [23]. The reduced stress (σ*) versus the reciprocity of the extension ratio (λ) for the X-SBR composites are illustrated in Fig. 5. Because of the

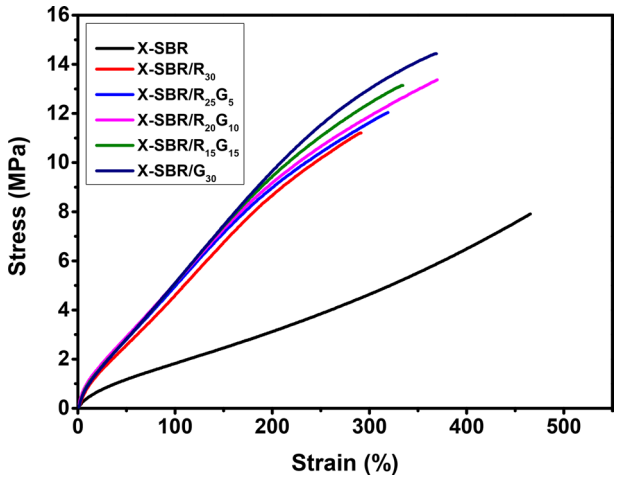

Fig. 4. Stress-strain curves of X-SBR, X-SBR/R_{30}, X-SBR/$R_{25}G_5$, X-SBR/$R_{20}S_{10}$, X-SBR/$R_{15}G_{15}$ and X-SBR/G_{30}.

Table 3. Mechanical properties of the X-SBR composites

Sample	X-SBR	X-SBR/R_{30}	X-SBR/$R_{25}G_5$	X-SBR/$R_{20}G_{10}$	X-SBR/$R_{15}G_{15}$	X-SBR/G_{30}
Hardness (shore A)	70	78	80	81	83	80
Modulus at 100% (MPa)	1.83	4.63	4.98	5.11	5.22	5.10
Tensile strength (MPa)	7.90	11.20	12.04	13.37	13.14	14.43
Elongation at break (%)	465	291	319	369	334	368

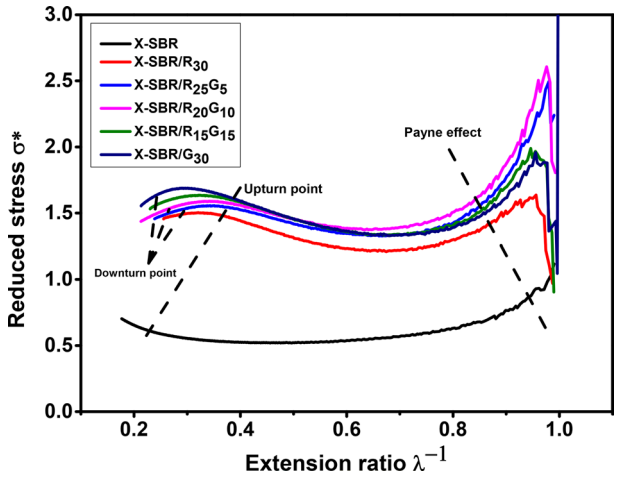

Fig. 5. Mooney-Rivlin plots of X-SBR, X-SBR/R_{30}, X-SBR/$R_{25}G_5$, X-SBR/$R_{20}S_{10}$, X-SBR/$R_{15}G_{15}$ and X-SBR/G_{30}.

Payne effect, σ* decreases during stretching at small extension ratios ($\lambda^{-1} > 0.8$). Notably, an upturn in σ* can be observed for the X-SBR composites; this observation indicates the strongest interaction between the filler and matrix, which favored the chain orientation when deformation was applied. It is significant to realize the chain orientation in rubber composites for rubber reinforcement [24]. However, for the X-SBR composites, the downturn point occurred at high extension ratios. It was accepted that the poor interfacial bonding resulted in these observed downturn behaviors. Thus, the Mooney–Rivlin plots proves that the interfacial bonding was gradually deteriorated with the increased particle loading. This may possibly be due to a high proportion of the fillers forming aggregations, which affected the uneven stress distribution. Another hypothesis is that when the extension ratio reached a certain value, the filler-matrix bond would break down [25].

3.5. Dynamic rheological properties of the X-SBR compounds

Dynamic rheological measurement with strain sweep of the X-SBR compounds was performed to analyze the filler network structure in the composites using the RPA2000 at 60°C and 1.67 Hz. The relationship between the storage modulus (G´) and strain are shown in Fig. 6, in which the dependence of the storage modulus on the strain can be seen. As the strain amplitude increased, the storage modulus decreased (which is widely known as the Payne effect) [26]. By comparing the neat X-SBR with the X-SBR composites, the neat X-SBR showed that the initial storage modulus was relatively low and did not exhibit any significant changes. In this case, individually adding either the RBC or graphite filler into the X-SBR matrix led to a larger storage modulus at smaller strains. It can be observed that X-SBR in the presence of RBC or graphite can be effectively enhanced. This revealed the formation of the filler network. In terms of the hybrid filler systems, X-SBR/$R_{25}G_5$, X-SBR/$R_{20}G_{10}$ and X-SBR/$R_{15}G_{15}$, as the graphite content was increased, the initial modulus of the compound appeared to further increase.

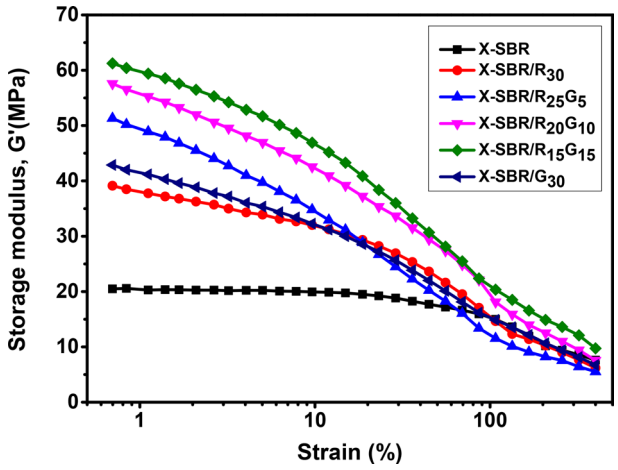

Fig. 6. Dynamic strain sweep of X-SBR, X-SBR/R_{30}, X-SBR/$R_{25}G_5$, X-SBR/$R_{20}S_{10}$, X-SBR/$R_{15}G_{15}$ and X-SBR/G_{30}.

In particular, X-SBR/$R_{15}G_{15}$ had the highest initial modulus, which means a significant Payne effect and implies that the filler network of the X-SBR was strong. It shows that RBC and graphite have a synergistic effect in reinforcing the network. This confirms that the presence of a strongly developed network of fillers in the polymer matrix contributes to its reinforcing character. This fact corroborates the analysis results of the vulcanization properties. It has been well documented that filler networks can be classified into three types: flexible, rigid, and mixed [27]. In this work, the filler network of the X-SBR/R_{30} and X-SBR/G_{30} composites were of the mixed variety while the filler network of the hybrid filler with RBC and graphite were of the rigid variety, in which the particles interact with each other directly leading to a higher initial storage modulus.

3.6. Abrasion resistance

The abrasion test of the vulcanizates was performed to measure wear loss with a Taber abrasion tester, and the wear loss was recorded at both 500 and 1000 cycles of rubbing for

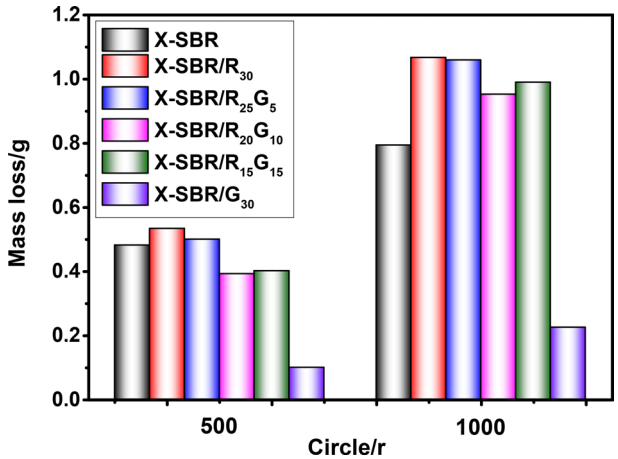

Fig. 7. Abrasion test results of X-SBR, X-SBR/R_{30}, X-SBR/$R_{25}G_5$, X-SBR/$R_{20}S_{10}$, X-SBR/$R_{15}G_{15}$ and X-SBR/G_{30}.

each specimen to calculate the different mass losses of the samples; the results are given in Fig. 7. It is accepted that abrasion resistance tests can be used to evaluate the service lifetime and safety of tires. As seen in the figure, the neat X-SBR has good abrasion resistance due to its nature. The composites that incorporated RBC had an inferior abrasion resistance compared with the composites that had incorporated graphite. It was also found that as the graphite content was increased in the hybrid system, the abrasion resistance of the composites improved to some extent. This shows that the strong interaction could have contributed to the improvement of the abrasion resistance of the composites [28]. Surprisingly, the composite X-SBR/G_{30} showed a much more outstanding abrasion resistance because of the better reinforcement and higher crosslink density. This phenomenon is in agreement with the work by Choi et al. [29].

3.7. Thermal properties of the X-SBR composites

The thermal property of the X-SBR composites was analyzed by thermogravimetric analysis (TGA). The weight loss and its derivative curves of the X-SBR composites measured in a N_2 atmosphere are compared in Fig. 8. From the TGA curves, it can be seen that the thermal decomposition temperature of the RBC and graphite were 421 and 635°C, respectively. At 800°C, the residue of the RBC and graphite tended to be 29 and 46%, respectively. Graphite as a reinforcing agent revealed a better thermal stability. Overall, a similar general shape was observed for the degradation of the X-SBR composites. Compared with the X-SBR composites, the neat X-SBR exhibited a poor thermal stability, implying a strong interaction between the fillers and the matrix which ensured an improvement in the thermal properties. As described in the inset of Fig. 8, the hybrid filler based on the RBC and graphite was incorporated into the X-SBR, and the initial decomposition temperature values increased with the increasing incorporation of the graphite contents. As a result, X-SBR/$R_{15}G_{15}$ had a higher initial decomposition temperature, which was attributed to its graphitic properties [30].

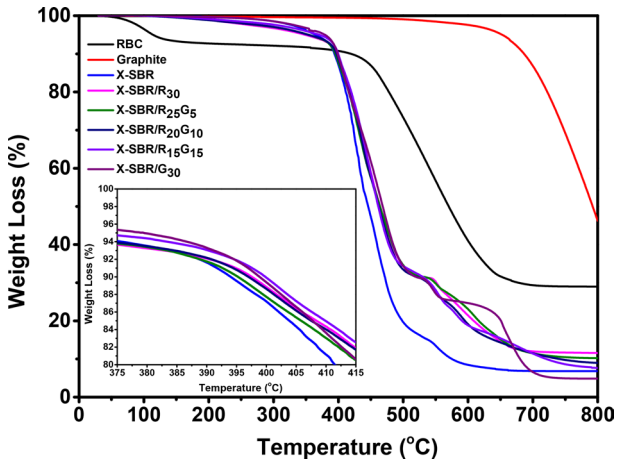

Fig. 8. TG curves of X-SBR, X-SBR/R_{30}, X-SBR/$R_{25}G_5$, X-SBR/$R_{20}S_{10}$, X-SBR/$R_{15}G_{15}$ and X-SBR/G_{30}.

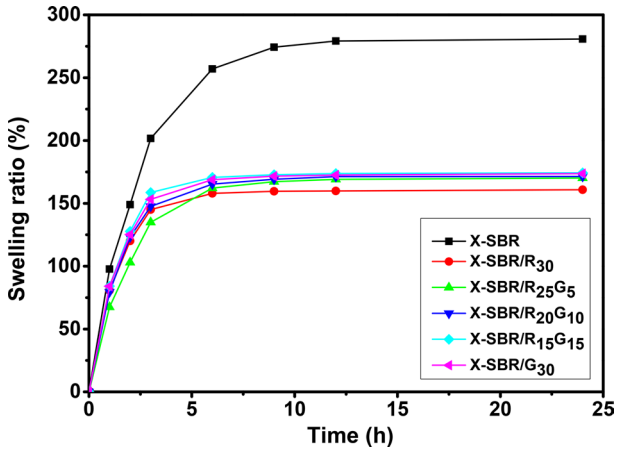

Fig. 9. Swelling ratio of X-SBR, X-SBR/R_{30}, X-SBR/$R_{25}G_5$, X-SBR/$R_{20}S_{10}$, X-SBR/$R_{15}G_{15}$ and X-SBR/G_{30}.

3.8. Swelling Properties of the X-SBR composites

In the swelling test, the swelling curves of the vulcanized neat X-SBR and X-SBR composites were determined. As shown in Fig. 9, the swelling ratio of the vulcanized neat X-SBR was 280%, which was much higher than that of the X-SBR composites. As expected, it easily expanded in the organic solvent due to its low crosslinking density and hydrophobicity. Apparently, RBC, graphite, and its hybrid fillers were added during the preparation because the reduction in the volume fraction of the rubber results in a decreased swelling ratio. X-SBR/R_{30} had a lower swelling ratio (160%) compared with X-SBR/G_{30} (173%), showing a better dispersion of RBC in the matrix. The effect of the different contents of graphite in the presence of RBC on the swelling of the X-SBR/RBC/graphite composites was also tested. It can also be seen that the composites containing hybrid fillers had a similar swelling behavior to that of the X-SBR/G_{30} composites. The swelling degree of the vulcanized samples in the presence of graphite increased slowly with the increasing of the graphite content, which was related to an increase in the interaction between the fillers and the rubber molecular chain to reinforce the swelling resistance.

4. Conclusions

A simple latex method was used to prepare X-SBR composites containing RBC, graphite, and its hybrid fillers, for which RBC was used as the main filler and coupled with graphite as a secondary filler, with the aim to compare the mechanical, dynamic rheological, and thermal behaviors of X-SBR. The RBC and graphite acted as good reinforcing fillers for the X-SBR. Graphite as a reinforced filler showed excellent abrasion resistance and thermal properties. A hybrid filler (a combination of 20 phr RBC and 10 phr graphite) improved the mechanical properties, but no such synergism behavior was observed. The interaction between the filler and the X-SBR molecules was characterized with Fourier transform infrared, TGA and RPA; the results confirmed such networks are present in the polymer matrix, which ensured a reinforcing character.

DOI: http://dx.doi.org/10.5714/CL.2018.27.072

Conflict of Interest

No potential conflict of interest relevant to this article was reported.

References

[1] Saowapark T, Plao-le S, Chaichana E, Jaturapiree A. Role of eco-friendly molasses carbon powder as a filler in natural rubber vulcanizates. Mater Today Proc, **4**, 6450 (2017). https://doi.org/10.1016/j.matpr.2017.06.152.

[2] Nanda M, Tripathy DK. Physico-mechanical and electrical properties of conductive carbon black reinforced chlorosulfonated polyethylene vulcanizates. eXPRESS Polym Lett, **2**, 855 (2008). http://doi.org/10.3144/expresspolymlett.2008.100.

[3] Lee SE, Cho S, Lee YS. Mechanical and thermal properties of MWCNT-reinforced epoxy nanocomposites by vacuum assisted resin transfer molding. Carbon Lett, **15**, 32 (2014). https://doi.org/10.5714/cl.2014.15.1.032.

[4] Jin FL, Lee SY, Park SJ. Polymer matrices for carbon fiber-reinforced polymer composites. Carbon Lett, **14**, 76 (2013). http://doi.org/10.5714/CL.2013.14.2.076.

[5] Kueseng K, Jacob KI. Natural rubber nanocomposites with SiC nanoparticles and carbon nanotubes. Eur Polym J, **42**, 220 (2006). https://doi.org/10.1016/j.eurpolymj.2005.05.011.

[6] Mao Y, Wen S, Chen Y, Zhang F, Panine P, Chan TW, Zhang L, Liang Y, Liu L. High performance graphene oxide based rubber composites. Sci Rep, **3**, 2508 (2013).

[7] Kim H, Abdala AA, Macosko CW. Graphene/polymer nanocomposites. Macromolecules, **43**, 6515 (2010). https://doi.org/10.1021/ma100572e.

[8] Liu Z, Zhang Y. Enhanced mechanical and thermal properties of SBR composites by introducing graphene oxide nanosheets decorated with silica particles. Composites Part A Appl Sci Manuf, **102**, 236 (2017). https://doi.org/10.1016/j.compositesa.2017.08.005.

[9] Lin Y, Liu S, Peng J, Liu L. The filler–rubber interface and reinforcement in styrene butadiene rubber composites with graphene/silica hybrids: a quantitative correlation with the constrained region. Composites Part A Appl Sci Manuf, **86**, 19 (2016). https://doi.org/10.1016/j.compositesa.2016.03.029.

[10] Song S, Zhang Y. Carbon nanotube/reduced graphene oxide hybrid for simultaneously enhancing the thermal conductivity and mechanical properties of styrene-butadiene rubber. Carbon, **123**, 158 (2017). https://doi.org/10.1016/j.carbon.2017.07.057.

[11] Lin Y, Chen Y, Zeng Z, Zhu J, Wei Y, Li F, Liu L. Effect of ZnO nanoparticles doped graphene on static and dynamic mechanical properties of natural rubber composites. Composites Part A Appl Sci Manuf, **70**, 35 (2015). https://doi.org/10.1016/j.compositesa.2014.12.008.

[12] Varghese TV, Kumar HA, Anitha S, Ratheesh S, Rajeev RS, Rao VL. Reinforcement of acrylonitrile butadiene rubber using pristine few layer graphene and its hybrid fillers. Carbon, **61**, 476 (2013). https://doi.org/10.1016/j.carbon.2013.04.104.

[13] Mondal S, Khastgir D. Elastomer reinforcement by graphene nanoplatelets and synergistic improvements of electrical and mechanical properties of composites by hybrid nano fillers of graphene-carbon black & graphene-MWCNT. Composites Part A Appl Sci Manuf, **102**, 154 (2017). https://doi.org/10.1016/j.compositesa.2017.08.003.

[14] Yan L, Zheng YB, Zhao F, Li S, Gao X, Xu B, Weiss PS, Zhao Y. Chemistry and physics of a single atomic layer: strategies and challenges for functionalization of graphene and graphene-based materials. Chem Soc Rev, **41**, 97 (2012). https://doi.org/10.1039/C1CS15193B.

[15] Wang R, Zhang J, Kang H, Zhang L. Design, preparation and properties of bio-based elastomer composites aiming at engineering applications. Compos Sci Technol, **133**, 136 (2016). https://doi.org/10.1016/j.compscitech.2016.07.019.

[16] Manocha LM, Warrier A, Manocha S, Banerji S, Sathiyamoorthy D. Mechanical properties of carbon/carbon composites densified by HIP technique. Carbon Lett, **6**, 6 (2005). http://carbonlett.org/PublishedPaper/topic_abstract.asp?idx=171.

[17] Zhang Y, Ge X, Li MC, Deng F, Oh J, Cho UR. The properties of rice bran carbon/nitrile-butadiene rubber composites fabricated by latex compounding method. Polym Compos, **39**, E687 (2016). https://doi.org/10.1002/pc.24126.

[18] Li MC, Zhang Y, Cho UR. Mechanical, thermal and friction properties of rice bran carbon/nitrile rubber composites: Influence of particle size and loading. Mater Des, **63**, 565 (2014). https://doi.org/10.1016/j.matdes.2014.06.032.

[19] Yin C, Zhang Q, Gong D. Preparation and properties of silica/styrene butadiene rubber masterbatches by latex co-coagulating technology. Polym Compos, **35**, 22770 (2013). https://doi.org/10.1002/pc.22770.

[20] Wang L, Zhao S. Study on the structure-mechanical properties relationship and antistatic characteristics of SSBR composites filled with SiO_2/CB. J Appl Polym Sci, **118**, 338 (2010). https://doi.org/10.1002/app.32372.

[21] D'Agostino A, Errico ME, Malinconico M, Rosa MD, Avella M, Schiraldi C. Development of nanocomposite based on hydroxyethylmethacrylate and functionalized fumed silica: mechanical, chemico–physical and biological characterization. J Mater Sci, **22**, 481 (2011). https://doi.org/10.1007/s10856-010-4223-1.

[22] Mooney M. A theory of large elastic deformation. J Appl Phys, **11**, 582 (1940). https://doi.org/10.1063/1.1712836.

[23] Zhang Y, Fei D, Xin G, Cho UR. Surface modification of novel rice bran carbon functionalized with (3-mercaptopropyl) trimethoxysilane and its influence on the properties of styrene-butadiene rubber composites. J Compos Mater, **50**, 2987 (2016). https://doi.org/10.1177/0021998315615202.

[24] Wang Z, Liu J, Wu S, Wang W, Zhang L. Novel percolation phenomena and mechanism of strengthening elastomers by nanofillers. Phys Chem Chem Phys, **12**, 3014 (2010). https://doi.org/10.1039/B919789C.

[25] Zhang Y, Ge X, Deng F, Li MC, Cho UR. Fabrication and characterization of rice bran carbon/styrene butadiene rubber composites fabricated by latex compounding method. Polym Compos, **38**, 2594 (2015). https://doi.org/10.1002/pc.23852.

[26] Payne AR, Whittaker RE, Smith JF. Effect of vulcanization on the low-strain dynamic properties of filled rubbers. J Appl Polym Sci, **16**, 1191 (1972). https://doi.org/10.1002/app.1972.070160513.

[27] Wang L, Ning N, Zhang L, Lu Y, Tian M, Chan T. Filler dispersion evolution of acrylonitrile-butadiene rubber/graphite nanocomposites during processing. Composites Part A Appl Sci Manuf, **47**, 135 (2013). https://doi.org/10.1016/j.compositesa.2012.12.004.

[28] Choi SS. Improvement of properties of silica-filled natural rubber compounds using polychloroprene. J Appl Polym Sci, **83**, 2609 (2002). https://doi.org/10.1002/app.10201.
[29] Choi SS, Park BH, Song H. Influence of filler type and content on properties of styrene-butadiene rubber (SBR) compound reinforced with carbon black or silica. Polym Adv Technol, **15**, 122 (2004). https://doi.org/10.1002/pat.421.
[30] Lee SM, Kang DS, Roh JS. Bulk graphite: materials and manufacturing process. Carbon Lett, **16**, 135 (2015). https://doi.org/10.5714/CL.2015.16.3.135.